# Chemical Analysis and Molecular Models for Calcium−Oxygen−Carbon Interactions in Black Carbon Found in Fertile Amazonian Anthrosoils

Braulio S. Archanjo,*[†] Joyce R. Araujo,[†] Alexander M. Silva,[†] Rodrigo B. Capaz,[†,‡] Newton P. S. Falcão,[†,§] Ado Jorio,[∥] and Carlos A. Achete[†,#]

[†]Instituto Nacional de Metrologia, Qualidade e Tecnologia, Av. Nossa Sra. das Graças, 50, 25250-020 Duque de Caxias, Rio de Janeiro, Brazil

[‡]Instituto de Física, Universidade Federal do Rio de Janeiro, Caixa Postal 68528, Rio de Janeiro, RJ 21941-972, Brazil

[§]Departamento de Ciências Agronômicas, Instituto Nacional de Pesquisas da Amazônia, Manaus, Amazonas 69011-970, Brazil

[∥]Departamento de Física, ICEx, Universidade Federal de Minas Gerais, Belo Horizonte, Minas Gerais 30123-970, Brazil

[#]Departamento de Engenharia Metalúrgica e de Materiais, Universidade Federal do Rio de Janeiro, Rio de Janeiro, RJ 21941-972, Brazil

**ⓢ** *Supporting Information*

**ABSTRACT:** Carbon particles containing mineral matter promote soil fertility, helping it to overcome the rather unfavorable climate conditions of the humid tropics. Intriguing examples are the Amazonian Dark Earths, anthropogenic soils also known as "Terra Preta de Índio" (TPI), in which chemical recalcitrance and stable carbon with millenary mean residence times have been observed. Recently, the presence of calcium and oxygen within TPI-carbon nanoparticles at the nano- and mesoscale ranges has been demonstrated. In this work, we combine density functional theory calculations, scanning transmission electron microscopy, energy dispersive X-ray spectroscopy, Fourier transformed infrared spectroscopy, and high resolution X-ray photoelectron spectroscopy of TPI-carbons to elucidate the chemical arrangements of calcium−oxygen−carbon groups at the molecular level in TPI. The molecular models are based on graphene oxide nanostructures in which calcium cations are strongly adsorbed at the oxide sites. The application of material science techniques to the field of soil science facilitates a new level of understanding, providing insights into the structure and functionality of recalcitrant carbon in soil and its implications for food production and climate change.
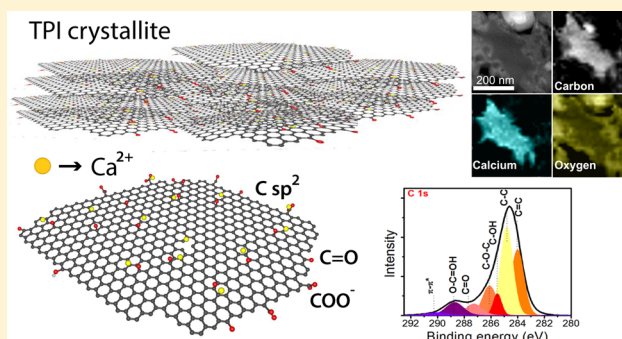
## INTRODUCTION

Soil organic matter (SOM) plays a fundamental role in soil biogeochemistry[1] and in carbon stored in soils.[2] A great deal of attention has been given to the most recalcitrant and stable forms of SOM, usually referred to as black carbon (BC), pyrolyzed biomass or, more recently, biochar.[1−4] The presence of stable carbon structures offers improved soil productivity,[1,5] further increasing biomass production. Furthermore, it has been claimed that sequestering carbon via low-temperature pyrolysis in soil is more efficient than the storage of carbon in plants and trees[1,2] because it increases the carbon mean residence time. One interesting and rather exotic example is the highly fertile anthropogenic soil found in the Amazonian region, known as "Terra Preta de Índio" (TPI) or Amazonian Dark Earth, which contains far more carbon than the surrounding soils.[3,6,7] In addition to their unusually high fertility over long periods of usage, TPI soils also present high resilience and stability, ranging from 600 to as much as 8700 years,[7] offering chemical recalcitrance even in the high temperature and humidity levels of the Amazonian climate.[5]

However, the reasons for the long residence times of carbon structures in soil are still under debate.[1,2,4,8−13] There is agreement that the partial oxidation of BC and fusing of the nonblack carbon based structures of SOM,[14,15] as well as its interaction with soil minerals,[1,8−12,14,16] are fundamental to its persistence in soil. In fact, studies[12,17,18] suggest that removing calcium from the soil increases SOM decomposition.

The presence of calcium and oxygen within TPI-carbon nanoparticles at the nano- and mesoscale ranges has been

demonstrated.[19] A nanoscale chemical mapping of an external region of a charcoal-like TPI-carbon grain showed that calcium is dissolved in the carbon-rich regions, while P, Si, Al, and Fe were found in the edges of the carbon-rich structures, showing the presence of mineral matter-SOM aggregation.[19] A prior study[20] examined the long-term transformation of biogenic calcium phosphate (e.g., animal bones) in TPI and reported that biogenic and crystalline Ca—P species convert into more soluble Ca—P phases over time. All these studies strongly encourage further investigations on the dissolution of calcium in soils and its interactions with carbon.

The objective of this study was to understand the energetics related to the stabilization of Ca and organic carbon in the soil. Using this rather unusual material, the TPI, we propose molecular models of calcium- and oxygen-rich carbon nanocrystallites based on spectroscopic chemical analyses and first-principles theoretical calculations. The chemical characterization is performed via Fourier transformed infrared spectroscopy (FTIR) and high resolution X-ray photoelectron spectroscopy (XPS) measurements, in which the calcium, carbon, and oxygen core—electron binding energies are studied in detail. The experimental results are then modeled by exploring different arrangements of $Ca^{2+}$ cations adsorbed on graphene oxide nanoclusters, considered here as theoretical models of TPI-carbon nanocrystallites.[19,21] The specific interactions of $Ca^{2+}$ with the carbon $\pi$-electron system and the most common oxide groups in the graphene oxide nanocluster are described. These findings provide new insights concerning the molecular structure of recalcitrant SOM, which is essential for understanding and reproducing the TPI fertility and resilience.

## ■ MATERIALS AND METHODS

**Samples.** The samples were prepared from TPI collected in Costa do Laranjal ($TPI_{CL}$), Manacapuru (Lat 3° 18′ S, Long. 60° 33′ W) in Amazonas State, Brazil. The samples were taken from the surface layer (0−20 cm depth) using a Dutch auger. Next, charcoal-like TPI-carbon grains were carefully selected with the help of optical microscope working at 5× magnification, and then macerated in an agate mortar and pestle following three filtering steps, with meshes of 75, 65, and 38 $\mu$m. The finest fraction was used for the XPS and FTIR studies.

The charcoal sample was produced in the Cellulose and Charcoal Laboratory at Instituto Nacional de Pesquisa da Amazônia (INPA) from Embaúba (*Cecropiahololeuca Miq.*), a native plant from the Amazonian region. The biomass was prepared from 3-year-old trees using the middle of the tree trunk of the central stem, avoiding the base and top fragments. The fresh material was then carbonized in a pyrolysis furnace of refractory bricks with a volume of 20 L. The furnace was brought to a temperature of 600 °C over a period of 2 h. When reaching the final temperature, the system was turned off and allowed to cool. The sample was then ground finely enough to pass through a 2 mm sieve.

Five different locations for each sample of TPI and charcoal were measured. The spectra did not show considerable changes (peak energies, fwhm or intensities), so that the results presented here are a faithful representations of the samples molecular structures.

**Scanning Transmission Electron Microscopy (STEM) and Energy Dispersive X-ray Spectroscopy (EDX).** Scanning transmission electron microscopy (STEM) and energy dispersive X-ray spectroscopy (EDX) microscopy were performed on a Cs-corrected FEI Titan 80/300 transmission electron microscope, equipped with a Gatan imaging filter Tridiem and an EDX analyzer. The elemental mappings were obtained by integrating characteristic X-ray signals during a drift-corrected STEM spectrum imaging experiment. STEM images were acquired using a high-angle annular dark-field detector.

**Fourier Transformed Infrared Spectroscopy (FTIR).** The FTIR analyses were performed in a PerkinElmer Spectrum GX spectrometer by the potassium bromide (KBr) transmission technique. The concentration of pellets tested was 1 mg of sample by 300 mg of KBr. The instrument resolution is nominally the three minimum steps, thus in this case, 3 cm$^{-1}$.

**X-ray Photoemission Spectroscopy (XPS).** The XPS analyses were performed in an ultrahigh vacuum medium (Omicron Nanotechnology) using a monochromatic Al K$\alpha$ ($h\nu$ = 1486.7 eV, resolution 0.3 eV) X-ray source for acquisition of high resolution peaks and Al nonmonochromatic ($h\nu$ = 1486.7 eV, resolution 0.8 eV) for acquisition of survey spectrum, and power was provided by emission of 16 mA at a voltage of 12.5 kV. The TPI-carbon survey spectra were obtained with an analyzer pass energy of 50 eV and steps of 0.8 eV. For calcium, carbon, and oxygen, the high energy resolution spectra were obtained with an analyzer pass energy of 30 eV and steps of 0.05 eV.

Calibration of the spectra was performed by setting the binding energy of the carbon 1s level of a neat graphite sample to 284.6 eV.

The peak fitting were completed by considering the peak areas evaluated by the CasaXPS software and the sensibility factor of each atom. As routinely applied to XPS analyses, a mixture of Gauss/Lorentz functions (70/30) and Shirley background were used in a least-squares routine for peak fitting. For fitting the high-resolution XPS spectrum of Ca, the doublet separation of 3.5 eV was used (Ca 2p$_{1/2}$ and Ca 2p$_{3/2}$). This choice is consistent with the XPS database for calcium ions and resulted in a fwhm of approximately 1.0 eV for each peak (see Supporting Information (SI) for details). For fitting C 1s peaks, the full width at half-maximum (fwhm) value was fixed at a maximum limit of 1 eV for all peaks as a starting parameter. The sp$^2$ peak of the C 1s envelope centered at 284.3 eV had a fwhm of 1.0 ± 0.2 eV. In addition, near to the sp$^2$ graphite component at 284.3 eV, we found at least three broad components to account for the overlapping C 1s features. It was found that the bands appearing at the higher energy region tended to be much broader (fwhm ≈ 1.7 eV) than the sp$^2$ component. In particular, the fwhm of the components at the tail of the C 1s envelopes tended to be approximately 2 eV.

**Computational Methods.** The adsorption energies and electronic structures of the molecules studied in this work are calculated using a fully quantum-mechanical approach in which electron−electron interactions are described by density functional theory (DFT) using the Gaussian 09 suite of programs. All structures were fully geometrically optimized without any constraints at the B3LYP/6-31(d,p) level of theory. Equilibrium geometries were verified by the presence of all-real frequencies in the vibrational spectrum. This methodology provides binding energies with average uncertainties of ±2 kcal/mol for systems in which noncovalent interactions prevails. More details about the computational methods are presented in the SI.

## ■ RESULTS AND DISCUSSION

A STEM image of a typical nanometer-sized carbon particle extracted from the external region of the TPI-grain is shown in Figure 1a. The particle surface is formed by smaller structures,
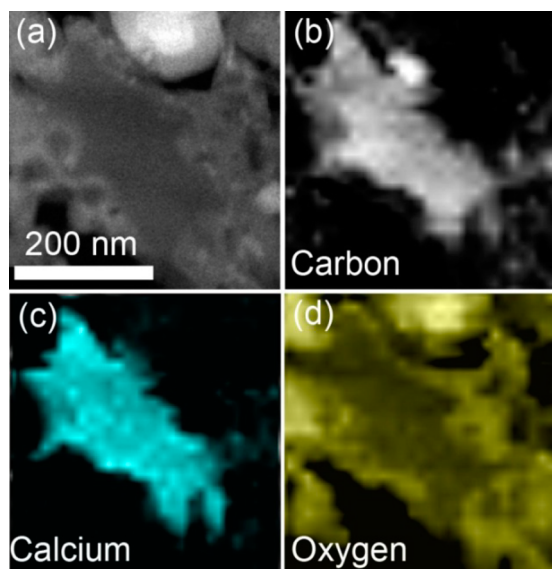


**Figure 1.** Scanning Transmission Electron Microscopy (STEM) and Energy Dispersive X-ray Spectroscopy (EDX) mapping of TPI-carbon grain, showing: (a) STEM image of the grain, (b) carbon, (c) calcium, and (d) oxygen chemical elemental maps.

which are several tens to hundreds of nanometers in length. Figure 1b−d shows EDX microscopic mapping sequence for carbon, calcium, and oxygen elements. The carbon rich region is observed at the core of TPI-carbon grain, Figure 1b. The calcium atoms are dissolved in the carbon region (Figure 1c),

indicating the presence of chemical interactions between calcium and carbon atoms that is evaluated in this work through spectroscopic techniques and theory. The oxygen atoms appear in all regions of the TPI-carbon grain (Figure 1d), but its concentration is higher on the border, which is consistent with the oxidation mechanism of soil organic matter where the oxygen atoms first react with the surface layer, and thereafter, diffuse into the TPI-grain.[17,19] Some authors report that an SOM oxidation mechanism occurs via an abiotic redox reaction involving SOM and a redox partner, e.g., $Fe^{3+}$, $Al^{3+}$, $Cu^{3+}$, $Zn^{2+}$, or $O_2$, that can be reduced to $H_2O_2$.[22] Such as oxygen atoms, these metals are located on the border of the TPI-carbon crystallite, thus favoring the SOM oxidation.

FTIR spectra of TPI and charcoal are shown in Figure 2. TPI spectrum shows band characteristics of aromatic C bounded to calcium and phosphorus elements (see all peak assignments in Table S2 in the SI). The most intense bands are in regions: 3405 $cm^{-1}$ (in-phase symmetric stretching O—H vibration), 3100 $cm^{-1}$ (aromatic =C—H stretching), 1600 $cm^{-1}$ (aromatic C=C stretching), 1000−1100 ($\nu_3$ $PO_4^{3-}$), 1415, and 870 $cm^{-1}$ (Ca—C—O/P—O—C aromatic stretching), and 607 $cm^{-1}$ (aryl phosphates).[23] The bands at 600 and 571 $cm^{-1}$ are assigned to components of the triply degenerate $\nu_4$ O—P—O bending mode, and the bands in the range 462−474 $cm^{-1}$ are assigned to the components of the doubly degenerate $\nu_2$ O—P—O bending mode. In contrast with TPI FTIR spectrum, charcoal spectrum shows essentially bands characteristics of aromatic compounds, and some of those overlap with bands found in TPI spectrum. The C—C stretching vibrations of conjugated ring occurs at 1570 $cm^{-1}$, a number of weak combination and overtones appear at ~1690 $cm^{-1}$, and finally, several bands are seen in the region between 900 and 600 $cm^{-1}$, which are related to different numbers of adjacent hydrogen atoms in the aromatic rings. In the present case, the three bands (880, 815, and 750 $cm^{-1}$) indicate a meta-disubstituted
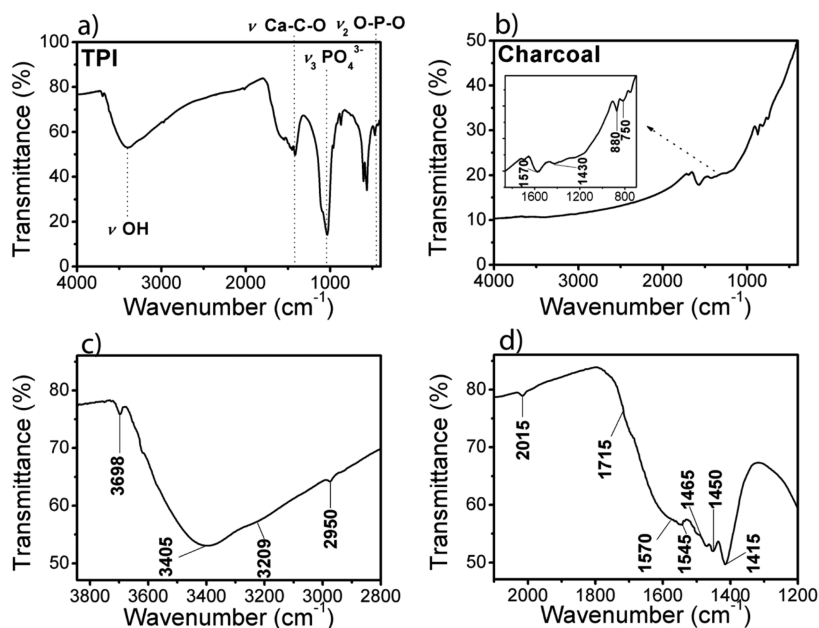


**Figure 2.** Chemical characterization of (a) the "Terra Preta de Índio" carbon nanostructures (TPI-carbons) and (b) charcoal using Fourier transformed infrared spectroscopy (FTIR). (c) and (d) show zooms of specific energy ranges for the TPI spectrum. In contrast to charcoal, which essentially shows only aromatic C=C molecular vibrations, the TPI-carbons spectrum shows Ca—C—O stretching modes and aryl phosphates stretching vibrations.

benzene.[23] A very weak band in 1430 cm$^{-1}$ is also indicative of disubstituted ring. The reader is referred to the SI for a more detailed discussion of these results.

Broad surveys of TPI-carbons and charcoal XPS spectra are shown in Figure 3. It is evident that the TPI-carbons show a
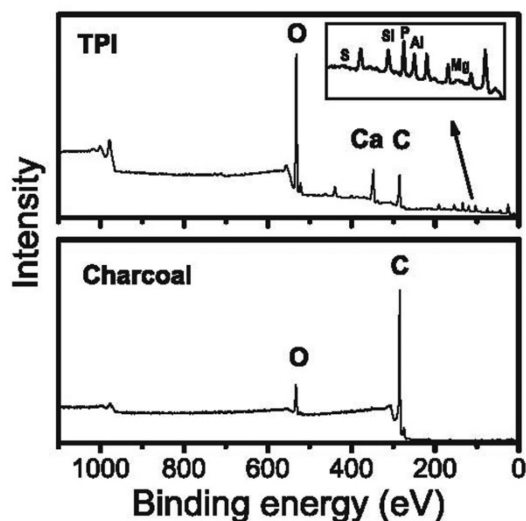


**Figure 3.** Chemical characterization of the "Terra Preta de Índio" carbon nanostructures (TPI-carbons, top) and charcoal (bottom) using X-ray photoelectron spectroscopy (XPS). In contrast to charcoal, which essentially shows only carbon and oxygen, the TPI-carbons show a rich variety of elements, as indicated near the associated XPS peaks.

variety of elements in their composition, in contrast to charcoal, which shows essentially only C and O. Similar to other productive soils,[24] the TPI-carbon spectrum shows the presence of Ca, P, Al, Mg, Si, and Na, as well as other elements with contents smaller than 1% (S, N, K, Ti, Cr, Mn, Fe, and Zn). In particular, the presence of Ca and P in the TPI-carbons has been attributed to bone fragments and animal residue.[25] From the XPS spectra, the core–electron binding energies of the elements found in TPI-carbons can be extracted. The binding energies are consistent with those obtained in silicates (P, Si), metallic oxides (Al, Ca, P, Fe) and metals adsorbed onto clayey materials (Mg, Ca, P).[24]

Detailed high resolution XPS analyses of the chemical groups in the TPI-carbons and charcoal containing carbon and oxygen are shown in Figure 4. The electron binding energies of carbon 1s (C 1s, Figure 4a) are assigned to the functional groups usually found in soil organic carbon, i.e. sp$^2$ hybridized carbon (C sp$^2$), epoxide and hydroxyl, carbonyl, carboxylate, and carbonate anions.[26] The electron binding energies of oxygen 1s (O 1s, Figure 4b) are less resolved and are generally attributed to oxidized carbon and metal oxides.[27−31]

The C 1s and O 1s XPS peaks of charcoal show only two major components,[27] whereas the TPI-carbons show more complex spectra. Oxidized carbon species comprise 62% of the TPI-carbons, while the remaining 38% consists of sp$^2$ carbon.[28] For the charcoal sample, the ratio of sp$^2$ carbon to oxidized carbon species is much larger than in the TPI-carbons: 73% sp$^2$ carbon to 27% oxidized carbon species.

The highest fractions of carbon–oxygen bonding in TPI-carbons are from epoxide (C—O—C) and hydroxyl (C—OH) groups.[29] Carbonyl (C=O) and carboxylate groups (COO$^-$)
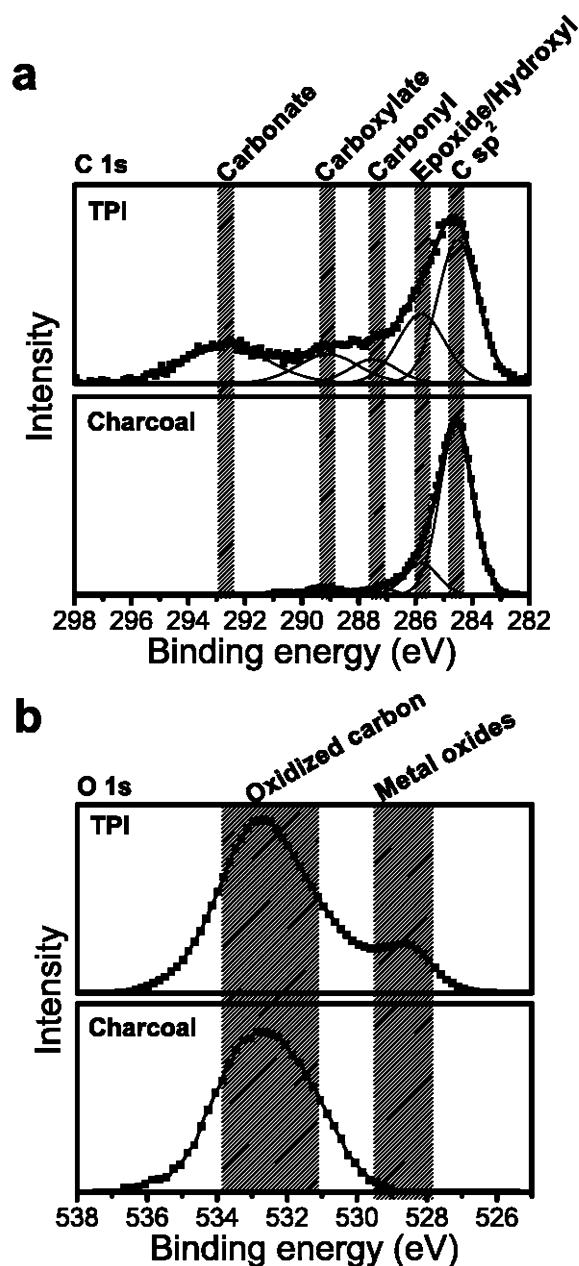


**Figure 4.** Molecular identification of (a) carbon and (b) oxygen in the TPI-carbons and charcoal, using high resolution X-ray photoelectron spectroscopy (XPS). The C 1s peaks are assigned as sp$^2$-hybridized carbon (C sp$^2$) at 284.5 eV, unresolved epoxide (C—O—C) and hydroxyl (C—OH) at 285.8 eV, carbonyl (C=O) at 287.5 eV, carboxylate groups (COO$^-$) at 289.1 eV, and carbonate ion (CO$_3^{2-}$) at 292.7 eV.[27−31] For the O 1s peaks, unresolved epoxy/carbonate, epoxide, and hydroxyl (components at 533.8, 532.6, and 531.0 eV, respectively) are generally attributed to "oxidized carbon". The O 1s peak appearing at 528.5 eV is attributed to oxygen−metal bonds.[28]

are known to be located at the edges of carbon crystallites.[27−30] The O 1s peak appearing at 528.5 eV is attributed to oxygen−metal bonds, as it is also present in calcium oxide.[31]

We now analyze in detail the XPS peaks associated with calcium in the TPI-carbons. Figure 5 shows that Ca is present in at least five different configurations, corresponding to Ca 2p$_{3/2}$ peaks at 345.6, 346.2, 346.8, 347.4, and 348.0 eV. These are assigned in Table 1 to, respectively, calcium bound to oxygen, calcium ionically bound to hydroxyl,[32] calcium bound

Ca 2p

TPI

*Ca-C sp²*
*Ca-phosphate*
*Ca- oxidized carbon*
*Ca-hydroxyl*
*Ca-oxygen*

Intensity

Binding energy (eV)
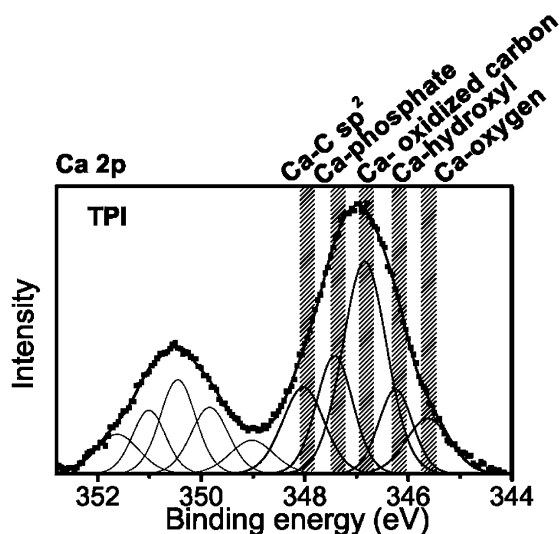
352  350  348  346  344

**Figure 5.** Identification of calcium chemical environments in the TPI-carbon, using high resolution X-ray photoelectron spectroscopy (see the SI for details). The electron binding energies of Ca $2p_{1/2}$ and Ca $2p_{3/2}$ are examined. The dominant peak is assigned to calcium bound to different forms of oxidized carbon, such as epoxide, carbonyl, and carboxylate groups. The presence of calcium oxygen, calcium-hydroxyl, calcium phosphate ($Ca_3(PO_4)_2$ and $CaHPO_4$) and calcium phys-isorbed on $sp^2$ carbon (Ca—C $sp^2$) are also observed.

to oxidized carbon, calcium-phosphate ($Ca_3(PO_4)_2$ and $CaHPO_4$) in mineral form,[20,33,34] and Ca cations physisorbed on $\pi$-clouds of $sp^2$ carbon (Ca—C $sp^2$).[35] The component at 346.8 eV is the highest peak and is assigned to calcium bound to different forms of oxidized carbon atoms, such as carboxylate anions, carbonyl and epoxide groups.[13,36] In Ca 2p XPS peak, $CaCO_3$ normally appears in the region of 346−347 eV, region where peaks coming from other forms of calcium overlap, such as calcium oxide, calcium hydroxide, calcium phosphate, and calcium bounded to oxidized carbon atoms in inner sphere complexes. In soil, $CaCO_3$ originates from mineral phase and has alkaline character (basic pH range).[37] In contrast, at the typical pH of TPI soil, humic substances are one the mostly important forms present in oxidized carbon region and responsible to the fertility, being composed by carboxyl groups directly attached to aromatic structure, making the pH of TPI-carbon in the acid pH range (between 3 and 5).

To understand these experimental results at the atomic and molecular levels, we performed theoretical calculations based on density functional theory. These techniques have recently been successfully applied in the field of soil science.[13,38,39] The presence of the above-mentioned chemical groups indicates the similarity, at the molecular level, between the TPI-carbons and graphene oxide.[40,41] It is well-known that the most common oxide groups in graphene oxide are the epoxide and hydroxyl groups in the basal plane and the carboxyl group (and possibly some hydroxyl and carbonyl groups) at the crystallite edges.[40,41] We explored this similarity to construct simplified theoretical models for the TPI-carbons. A graphene nanocluster ($C_{54}H_{18}$ molecule) was then used as a host for various oxygen chemical groups and $Ca^{2+}$, making it possible to study their interactions.

The different chemical interactions between calcium and oxidized carbon were studied by considering six different configurations. All adsorption energy values obtained via our theoretical calculations are displayed in Table 1, together with the calculated and experimental core−electron binding energies (discussed in the analysis of the XPS measurements). $Ca^{2+}$ adsorption energies onto graphene oxide nanoclusters were calculated as the difference between the total energy of the $Ca^{2+}$−GO complex and the sum of total energies of GO and $Ca^{2+}$.

The six models are described below:

(1) $Ca^{2+}$ adsorption in the middle of the basal graphene plane, as shown in Figure 6a. This model represents the ideal situation of $Ca^{2+}$ adsorption on pristine graphene. Our calculated adsorption energy is −121 kcal/mol, resulting from the interaction between the $Ca^{2+}$ cation and the $\pi$-electrons of the basal plane. This value agrees with that in a previous study.[19] The smallest Ca—C distance is 2.73 Å in this case.

(2) Interaction between $Ca^{2+}$ and epoxide groups, as shown in Figure 6b. The oxygen atom initially forms a "bridge" configuration between two neighboring carbon atoms. However, the $Ca^{2+}$ cation breaks one of the O—C bonds and binds strongly to the oxygen atom. The adsorption energy is −147 kcal/mol and the Ca—O distance is 2.15 Å. The enhancement in adsorption energy occurs because the $Ca^{2+}$ cation is now in a more electronegative environment and interacts simultaneously with the epoxide group and the $\pi$-electrons, clearly enhancing

## Table 1. Summary of the Chemical Interactions of Ca with C and O in TPI[a]

| chemical interaction | $Ca^{2+}$ adsorption energy (kcal/mol) | core−electron binding energy (eV) | | | | | |
| --- | --- | --- | --- | --- | --- | --- | --- |
| | | Ca $2p_{3/2}$ | | C 1s | | O 1s | |
| | | exp. | theory | exp. | theory | exp. | theory |
| Ca—C $sp^2$ | −121 | 348.0 | 351.1 | 284.5 | 283.8 | | |
| Ca—hydroxyl | −125 | 346.2 | 348.5 | 285.8 | 285.2 | 533.8 | 528.2 |
| Ca—carbonyl[b] | −126 | 346.8 | 348.9 | 287.5 | 285.1 | 532.6 | 526.0 |
| Ca—carboxyl[b] | −146 | | 351.2 | | 286.0 | | 527.1 |
| Ca—epoxide[b] | −147 | 346.8 | 348.3 | 285.8 | 285.7 | 533.8 | 527.7 |
| Ca—carboxylate[b] | −292 | 346.8 | 347.8 | 289.1 | 282.1 | 531.0 | 522.9 |
| Ca—phosphate | | 347.4 | | 292.7 | | 531.0 | |
| Ca—oxygen | | 345.6 | | | | 528.7 | |

[a]Calculated adsorption energies as well as experimental and calculated core-electron binding energies for Ca $2p_{3/2}$, C 1s, and O 1s (in the presence of Ca) are displayed. Ca-carboxyl is not observed experimentally because it is not stable with respect to removal of one proton and transformation to Ca-carboxylate, at typical soil pH conditions. Ca-phosphate and Ca oxygen are not calculated because they originate from minerals. [b]Chemical interactions corresponding to Ca bound to oxidized carbon.
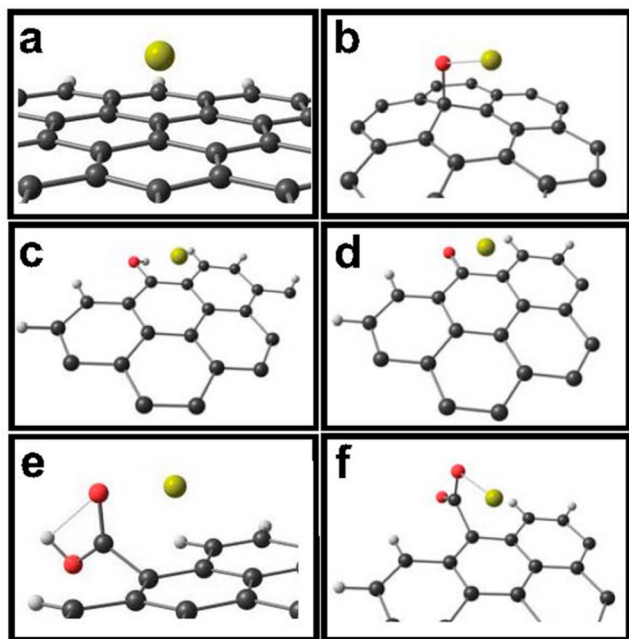
**Figure 6.** Atomic geometries for the different structures considered in this work: (a) Ca—C sp$^2$; (b) Ca—epoxide; (c) Ca—hydroxyl (edge); (d) Ca—carbonyl, (e); Ca—carboxyl; and (f) Ca—carboxylate. Carbon, hydrogen, oxygen, and calcium atoms are represented by black, white, red, and yellow balls, respectively. For clarity of the Ca sites, only part of the simulation cluster is shown in each case. For more details about the cluster, see the SI.

the electrostatic interaction. As shown below, the same enhancement occurs for calcium interactions with other oxygen-related chemical groups.

(3) Interaction between Ca$^{2+}$ and hydroxyl groups, as shown in Figure 6c. Interestingly, when the hydroxyl group is in the basal plane, the Ca$^{2+}$ binds very strongly to OH, removing it from the graphene oxide plane and then acting as a partial healer of the oxidized surface. Therefore, the hydroxyl—Ca$^{2+}$complex adsorbed on the basal plane is unstable. Most likely, a single Ca cation can remove two OH groups from the surface, thus forming Ca(OH)$_2$. However, if the hydroxyl group is placed at the crystallite edge, the Ca$^{2+}$ cation does not remove the OH group. The Ca$^{2+}$ cation actually binds to the OH group with adsorption energy of −125 kcal/mol, as shown in Figure 6c. The Ca—O distance is 3.70 Å, larger than in the epoxide case, which is consistent with the difference in adsorption energies in both cases.

(4) Interaction between Ca$^{2+}$ and a carbonyl group at the edge, as shown in Figure 6d. In this case, the adsorption energy is −126 kcal/mol and the Ca—O distance is 3.60 Å.

(5) Interaction between Ca$^{2+}$ cations and carboxyl groups at the graphene nanocluster edge, as shown in Figure 6e. The adsorption energy of the stable structure after geometrical optimization is −146 kcal/mol and the Ca—O distance is 2.39 Å. Ca—carboxyl may not be observed experimentally because it is not stable with respect to the removal of one proton and transformation to Ca—carboxylate under typical soil pH conditions.

(6) For the stable carboxylate anion, shown in Figure 6f, the electrostatic interaction with the Ca$^{2+}$ cation is even stronger, with adsorption energy of −292 kcal/mol. The

Ca—O distance is 2.21 Å. It is important to stress that, from a soil science perspective, it is well-known that carboxylate anions play an important role in fertility.[15] The presence of acid groups in TPI surfaces makes the carbon surfaces more hydrophilic and decreases the pH of the point of zero charge.

We also investigated structures containing more than one Ca$^{2+}$ cation per oxygen chemical group, but they were all unstable with respect to the desorption of the second cation. In other words, each of the chemical groups studied here could hold only one Ca$^{2+}$ cation and extra cations, if present, moved relatively freely through the TPI structure, which may have important implications for cation exchange considerations.

## ENVIRONMENTAL IMPLICATIONS

Approximately 2400 Pg of carbon is stored in soil profiles as soil organic matter.[42] A key issue with important environmental implications is the intermolecular associations between organic carbon and minerals or metal ions, which is one of the dominant mechanisms affecting the stability of soil organic carbon. It is known that Ca is among the most plentiful elements at the earth's surface, and the most abundant type of mineral cation in the soil. In addition, Ca can replace micronutrients (Fe and Zn) in chelates, forming calcium organometallic compounds. All these aspects make the analysis of C and Ca intermolecular associations important for envisioning how to control greenhouse gas emissions. At the same time, promoting a better soil fertility, thus increasing food production.

In this study, we addressed the C and Ca intermolecular associations by analyzing results found in a very special type of soil, the "Terra Preta do Índio" (TPI). In the Amazon forest, the soil organic carbon comprises 80 Mg C ha$^{-1}$ for sand soil, and 130 Mg C ha$^{-1}$ for clayey soils, always in the first one meter of dep.[43] In the TPI[44,45] specifically, the black carbon (or pyrogenic carbon, or biochar) is responsible for maintaining the high levels of soil organic matter and available nutrients, keeping fertility and recalcitrance high during long-term usage. Both the production and stability of this black carbon is tightly related to the high amounts of animal organic wastes, rich in Ca minerals that were dumped, buried, or burned during TPI formation.[46] Our calculations demonstrate strong chemical interaction of oxidized carbon and calcium in a specific molecular model, with adsorption energies as high as −292 kcal/mol per calcium cation. More importantly, the agreement between the calculated and experimental core—electron binding energies confirms the validity of our molecular models. These findings drive us toward the end goal of producing stable carbon structures that can be used for improving soil usage, with potential implications in agriculture and climate change.

## ASSOCIATED CONTENT

**S** Supporting Information

Detailed descriptions of fitting procedure of Ca 2p XPS peak; two tables listing XPS and FT-IR peak assignments; a figure showing a zoom of two regions of the TPI-FTIR spectrum; discussion about the FTIR bands and background observed in the charcoal spectrum; further details about the computational methods. This material is available free of charge via the Internet at http://pubs.acs.org.

## ■ AUTHOR INFORMATION

**Corresponding Author**

*Tel.: +55 21 26799021; fax: +55 21 26799597; e-mail: bsarchanjo@inmetro.gov.br.

**Notes**

The authors declare no competing financial interest.

## ■ REFERENCES

(1) Schmidt, M. W. I.; Torn, M. S.; Abiven, S.; Dittmar, T.; Guggenberger, G.; Janssens, I. A.; Kleber, M.; Kogel-Knabner, I.; Lehmann, J.; Manning, D. A. C.; Nannipieri, P.; Rasse, D. P.; Weiner, S.; Trumbore, S. E. Persistence of soil organic matter as an ecosystem property. *Nature* **2011**, *478* (7367), 49−56.

(2) Stockmann, U.; Adams, M. A.; Crawford, J. W.; Field, D. J.; Henakaarchchi, N.; Jenkins, M.; Minasny, B.; McBratney, A. B.; de Courcelles, V. D.; Singh, K.; Wheeler, I.; Abbott, L.; Angers, D. A.; Baldock, J.; Bird, M.; Brookes, P. C.; Chenu, C.; Jastrowh, J. D.; Lal, R.; Lehmann, J.; O'Donnell, A. G.; Parton, W. J.; Whitehead, D.; Zimmermann, M. The knowns, known unknowns and unknowns of sequestration of soil organic carbon. *Agric. Ecosyst. Environ.* **2013**, *164*, 80−99.

(3) Lehmann, J.; Solomon, D.; Kinyangi, J.; Dathe, L.; Wirick, S.; Jacobsen, C. Spatial complexity of soil organic matter forms at nanometre scales. *Nat. Geosci.* **2008**, *1* (4), 238−242.

(4) Ameloot, N.; Graber, E. R.; Verheijen, F. G. A.; De Neve, S. Interactions between biochar stability and soil organisms: Review and research needs. *Eur. J. Soil Sci.* **2013**, *64* (4), 379−390.

(5) Novotny, E. H.; Hayes, M. H. B.; Madari, B. E.; Bonagamba, T. J.; deAzevedo, E. R.; de Souza, A. A.; Song, G. X.; Nogueira, C. M.; Mangrich, A. S. Lessons from the Terra Preta de Indios of the Amazon Region for the utilisation of charcoal for soil amendment. *J. Braz. Chem. Soc.* **2009**, *20* (6), 1003−1010.

(6) Briones, A. The secrets of El Dorado viewed through a microbial perspective. *Front. Microbiol.* **2012**, *3* (239), 1−6.

(7) Liang, B.; Lehmann, J.; Solomon, D.; Kinyangi, J.; Grossman, J.; O'Neill, B.; Skjemstad, J. O.; Thies, J.; Luizao, F. J.; Petersen, J.; Neves, E. G. Black Carbon increases cation exchange capacity in soils. *Soil Sci. Soc. Am. J.* **2006**, *70* (5), 1719−1730.

(8) Torn, M. S.; Trumbore, S. E.; Chadwick, O. A.; Vitousek, P. M.; Hendricks, D. M. Mineral control of soil organic carbon storage and turnover. *Nature* **1997**, *389* (6647), 170−173.

(9) Brodowski, S.; John, B.; Flessa, H.; Amelung, W. Aggregate-occluded black carbon in soil. *Eur. J. Soil Sci.* **2006**, *57* (4), 539−546.

(10) Six, J.; Conant, R. T.; Paul, E. A.; Paustian, K. Stabilization mechanisms of soil organic matter: Implications for C-saturation of soils. *Plant Soil* **2002**, *241* (2), 155−176.

(11) Schimel, D. S.; Braswell, B. H.; Holland, E. A.; McKeown, R.; Ojima, D. S.; Painter, T. H.; Parton, W. J.; Townsend, A. R. Climatic, edaphic, and biotic controls over storage and turnover of carbon in soils. *Global Biogeochem. Cycles* **1994**, *8* (3), 279−293.

(12) Oades, J. M. The retention of organic-matter in soils. *Biogeochemistry* **1988**, *5* (1), 35−70.

(13) Keiluweit, M.; Kleber, M. Molecular-level interactions in soils and sediments: The role of aromatic $\pi$-systems. *Environ. Sci. Technol.* **2009**, *43* (10), 3421−3429.

(14) Kogel-Knabner, I.; Ekschmitt, K.; Flessa, H.; Guggenberger, G.; Matzner, E.; Marschner, B.; von Luetzow, M. An integrative approach of organic matter stabilization in temperate soils: Linking chemistry, physics, and biology. *J. Plant Nutr. Soil Sci.* **2008**, *171* (1), 5−13.

(15) Ni, J.; Pignatello, J. J.; Xing, B. Adsorption of aromatic carboxylate ions to black carbon (biochar) is accompanied by proton exchange with water. *Environ. Sci. Technol.* **2011**, *45* (21), 9240−9248.

(16) Schmidt, M. W. I.; Noack, A. G. Black carbon in soils and sediments: Analysis, distribution, implications, and current challenges. *Global Biogeochem. Cycles* **2000**, *14* (3), 777−793.

(17) Mikutta, R.; Mikutta, C.; Kalbitz, K.; Scheel, T.; Kaiser, K.; Jahn, R. Biodegradation of forest floor organic matter bound to minerals via different binding mechanisms. *Geochim. Cosmochim. Acta* **2007**, *71* (10), 2569−2590.

(18) Morris, S. J.; Bohm, S.; Haile-Mariam, S.; Paul, E. A. Evaluation of carbon accrual in afforested agricultural soils. *Global Change Biol.* **2007**, *13* (6), 1145−1156.

(19) Jorio, A.; Ribeiro-Soares, J.; Cancado, L. G.; Falcao, N. P. S.; Dos Santos, H. F.; Baptista, D. L.; Ferreira, E. H. M.; Archanjo, B. S.; Achete, C. A. Microscopy and spectroscopy analysis of carbon nanostructures in highly fertile Amazonian anthrosoils. *Soil Tillage Res.* **2012**, *122*, 61−66.

(20) Sato, S.; Neves, E. G.; Solomon, D.; Liang, B. Q.; Lehmann, J. Biogenic calcium phosphate transformation in soils over millennial time scales. *J. Soils Sed.* **2009**, *9* (3), 194−205.

(21) Ribeiro-Soares, J.; Cancado, L. G.; Falcao, N. P. S.; Martins Ferreira, E. H.; Achete, C. A.; Jorio, A. The use of Raman spectroscopy to characterize the carbon materials found in Amazonian anthrosoils. *J. Raman Spectrosc.* **2013**, *44* (2), 283−289.

(22) Studenroth, S.; Huber, S. G.; Kotte, K.; Schöler, H. F. Natural abiotic formation of oxalic acid in soils: Results from aromatic model compounds and soil samples. *Environ. Sci. Technol.* **2013**, *47* (3), 1323−1329.

(23) Socrates, G. *Infrared and Raman Characteristic Group Frequencies: Tables and Charts*; Wiley: New York, 2001.

(24) Chiaa, C. H.; Munroe, P.; Joseph, S.; Lina, Y. Microscopic characterisation of synthetic Terra Preta. *Aust. J. Soil Res.* **2010**, *48* (6−7), 593−605.

(25) Arroyo-Kalin, M.; Neves, E. G.; Woods, W. I. Anthropogenic Dark Earths of the Central Amazon Region: Remarks on Their Evolution and Polygenetic Composition. In *Amazonian Dark Earths: Wim Sombroek's Vision*; Woods, W., Teixeira, W., Lehmann, J., Steiner, C., WinklerPrins, A., Rebellato, L., Eds.; Springer: Netherlands, 2009; pp 99−125.

(26) Cheng, C. H.; Lehmann, J.; Thies, J. E.; Burton, S. D.; Engelhard, M. H. Oxidation of black carbon by biotic and abiotic processes. *Org. Geochem.* **2006**, *37* (11), 1477−1488.

(27) Lin, Y.; Munroe, P.; Joseph, S.; Kimber, S.; Van Zwieten, L. Nanoscale organo-mineral reactions of biochars in ferrosol: An investigation using microscopy. *Plant Soil* **2012**, *357* (1−2), 369−380.

(28) Liang, B.; Lehmann, J.; Solomon, D.; Sohi, S.; Thies, J. E.; Skjemstad, J. O.; Luizao, F. J.; Engelhard, M. H.; Neves, E. G.; Wirick, S. Stability of biomass-derived black carbon in soils. *Geochim. Cosmochim. Acta* **2008**, *72* (24), 6069−6078.

(29) Larciprete, R.; Lacovig, P.; Gardonio, S.; Baraldi, A.; Lizzit, S. Atomic oxygen on graphite: Chemical characterization and thermal reduction. *J. Phys. Chem. C* **2012**, *116* (18), 9900−9908.

(30) Filik, J.; May, P. W.; Pearce, S. R. J.; Wild, R. K.; Hallam, K. R. XPS and laser Raman analysis of hydrogenated amorphous carbon films. *Diamond Relat. Mater.* **2003**, *12* (3−7), 974−978.

(31) Ji, X.; Chen, Y.; Zhao, G.; Wang, X.; Liu, W. Tribological properties of $CaCO_3$ nanoparticles as an additive in lithium grease. *Tribol. Lett.* **2011**, *41* (1), 113−119.

(32) Dahle, S.; Voigts, F.; Maus-Friedrichs, W. In situ preparation of calcium hydroxide films. *Thin Solid Films* **2011**, *520* (1), 18−24.

(33) Ohtsu, N.; Hiromoto, S.; Yamane, M.; Satoh, K.; Tomozawa, M. Chemical and crystallographic characterizations of hydroxyapatite- and octacalcium phosphate-coatings on magnesium synthesized by chemical solution deposition using XPS and XRD. *Surf. Coat. Technol.* **2013**, *218*, 114−118.

(34) Ide-Ektessabi, A.; Yamaguchi, T.; Tanaka, Y. RBS and XPS analyses of the composite calcium phosphate coatings for biomedical applications. *Nucl. Instrum. Methods Phys. Res. B* **2005**, *241* (1−4), 685−688.

(35) Wang, X.; Bai, H.; Jia, Y.; Zhi, L.; Qu, L.; Xu, Y.; Li, C.; Shi, G. Synthesis of CaCO₃/graphene composite crystals for ultra-strong structural materials. *RSC Adv.* **2012**, *2* (5), 2154−2160.

(36) Christie, A. B.; Lee, J.; Sutherland, I.; Walls, J. M. An XPS study of ion-induced compositional changes with group-II and group-IV compounds. *Appl. Surf. Sci.* **1983**, *15* (1−4), 224−237.

(37) Stevenson, F. J.; Cole, M. A. *Cycles of Soils: Carbon, Nitrogen, Phosphorus, Sulfur, Micronutrients*; Wiley: New York, 1999.

(38) Tunega, D.; Gerzabek, M. H.; Totsche, K. U. Advances of molecular modeling of biogeochemical interfaces in soils. *Geoderma* **2011**, *169*, 1−3.

(39) Kalinichev, A. G.; Iskrenova-Tchoukova, E.; Ahn, W. Y.; Clark, M. M.; Kirkpatrick, R. J. Effects of Ca²⁺ on supramolecular aggregation of natural organic matter in aqueous solutions: A comparison of molecular modeling approaches. *Geoderma* **2011**, *169*, 27−32.

(40) Lu, N.; Huang, Y.; Li, H.-b.; Li, Z.; Yang, J. First principles nuclear magnetic resonance signatures of graphene oxide. *J. Chem. Phys.* **2010**, *133*, (3).

(41) Lee, D. W.; De Los Santos, L. V.; Seo, J. W.; Felix, L. L.; Bustamante, D. A.; Cole, J. M.; Barnes, C. H. W. The structure of graphite oxide: Investigation of its surface chemical groups. *J. Phys. Chem. B* **2010**, *114* (17), 5723−5728.

(42) Brady, N. C.; Weil, R. R. *The Nature and Properties of Soils*; Prentice Hall/Pearson Education: Upper Saddle River, New Jersey, 2008.

(43) Moraes, J. L.; Cerri, C. C.; Melillo, J. M.; Kicklighter, D.; Neill, C.; Steudler, P. A.; Skole, D. L. Soil carbon stocks of the Brazilian Amazon Basin. *Soil Sci. Soc. Am. J.* **1995**, *59* (1), 244−247.

(44) Glaser, B.; Haumaier, L.; Guggenberger, G.; Zech, W. The 'Terra Preta' phenomenon: A model for sustainable agriculture in the humid tropics. *Naturwissenschaften* **2001**, *88* (1), 37−41.

(45) Lehmann, J.; Pereira da Silva, J., Jr.; Steiner, C.; Nehls, T.; Zech, W.; Glaser, B. Nutrient availability and leaching in an archaeological Anthrosol and a Ferralsol of the Central Amazon basin: fertilizer, manure and charcoal amendments. *Plant Soil* **2003**, *249* (2), 343−357.

(46) Myers, T.; Denevan, W.; Winklerprins, A.; Porro, A., Historical Perspectives on Amazonian Dark Earths. In *Amazonian Dark Earths*; Lehmann, J., Kern, D., Glaser, B., Wodos, W., Eds.; Springer: Netherlands, 2003; pp 15−28.